

引线间距对 QFP 焊点的可靠性影响的有限元分析

盛 重， 薛松柏， 张 亮， 皋利利
(南京航空航天大学 材料科学与技术学院 南京 210016)

摘 要: 采用有限元方法分别对具有相同引线间距和不同封装类型的 QFP 器件的焊点残余应力进行了数值模拟计算分析。结果表明, 焊点根部、焊趾部位以及引线和焊点交界处为应变集中区域, 该三处将可能成为焊点发生破坏区域, 在焊点根部的应力值是最大的, 所以在焊点根部最容易发生破坏。对结果进行分析比较, 从应力曲线图可以看出, 由于残余应力累积的原因, 应力具有迭加性; 在引线数目相同的 QFP 器件中, TQFP64 焊点的应力最小, VQFP64 次之, SQFP64 最大。在引线间距相同的 QFP 器件中, QFP64 焊点的应力最小, QFP44 居中, QFP32 最大; 同时与 QFP100 比较可知, 高密度细间距器件的焊点可靠性更高。

关键词: 有限元; 残余应力; 引线间距; 引线数

中图分类号: TG115.28 文献标识码: A 文章编号: 0253-360X(2008)05-0085-04



盛 重

0 序 言

随着表面组装(SMT)技术的不断完善, 尤其是随着电子封装的密度越来越高, 使用细间距引脚的器件成为一种主流。小外型封装 SOP (small outline package)、四方扁平封装 QFP (quad flat package) 以及 BGA (ball grid array) 等封装形式日益增多, 逐步占据主导地位, 但是在实际生产中 QFP 的使用更为普遍^[1]。QFP 是指外形为正方形或矩形, 四边具有翼形短引线的塑料薄形封装形式, 也指采用该种封装形式的器件^[2]。QFP 器件封装外形尺寸小, 适合高频应用, 适于大批量生产, 从而价廉物美, 虽然封装密度受到 BGA 的挑战, 但是 QFP 器件在电子工业中仍然占重要地位。

在微电子焊接中, 电子组件的体积正朝着微型化、超微型化的方向发展, 如此微小的尺寸, 给焊点可靠性的试验研究带来了一定的困难, 有限元模拟方法在此课题方面可以提供一定的理论依据。在焊点可靠性研究中, 由于基板和焊点的线膨胀系数不匹配, 在交变的温度循环中会产生交变的热应力, 致使焊点发生疲劳失效。已有研究表明^[3], 表面组装焊点在环境温度循环条件下的失效现象是导致电子

装连失效的主要原因。因此焊点可靠性的研究是表面组装的关键技术。

针对 QFP 引线间距及封装类型对器件焊点可靠性的影响, 选用 TQFP (thin quad flat package), SQFP (shorten quad flat package) 和 VQFP (very-fine quad flat package) 三种类型的器件为研究对象, 采用有限元方法进行了数值模拟, 可以为 QFP 器件焊点可靠性提供理论数据。

1 模型的建立和参数的选择

1.1 QFP 的实体模型和单元划分

分别选择相同引线间距与相同引线数目不同封装类型的 QFP 元器件为研究对象, 根据焊点材料以及引线的相关几何参数建立有限元模型。由于 QFP 器件的对称性, 所以可取其 1/4 建立有限元模型, 如图 1 所示, 模型由塑料基板、铜引线、焊点和 PCB 板

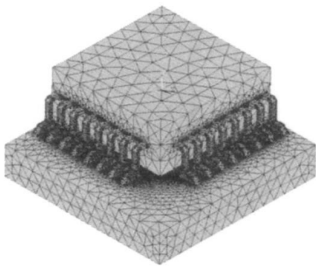


图 1 有限元模型
Fig 1 Finite element model

收稿日期: 2008-01-14
基金项目: 江苏省普通高校研究生科技创新计划资助项目(CX07B-087z); 2006 年江苏省“六大人才高峰”资助项目(06-E-020)

(FR-4)组成, 基板及引线尺寸如表 1 和表 2 所示。

表 1 不同类型器件尺寸

Table 1 Sizes of different types devices

器件	塑料基板 (mm×mm×mm)	宽度 <i>b</i> /mm	间距 <i>d</i> /mm	高度 <i>h</i> /mm
TQFP64	7×7×1	0.15	0.4	0.562 5
VQFP64	10×10×1.4	0.2	0.5	0.762 5
SQFP64	12×12×1.4	0.3	0.65	0.762 5

表 2 器件尺寸

Table 2 Sizes of devices

器件	塑料基板 (mm×mm×mm)	宽度 <i>b</i> /mm	间距 <i>d</i> /mm	高度 <i>h</i> /mm
QFP32	7×7×1.45	0.4	0.8	0.8
QFP44	10×10×2.15	0.35	0.8	1.15
QFP64	14×14×2.7	0.35	0.8	1.425
QFP100	20×14×2.45	0.3	0.5	1.3

建模采用自上而下和自下而上两种方法混合运用, 由于网格划分后, 整体模型的单元数过多, 给计算机的运算带来了困难。为了节省时间, 采用部分模型代替整体的方法, 如图 2 所示。整个模型采用四面体网格单元, 其中焊点采用粘塑性单元 Visco Solid107, 其它部分采用 Solid45 单元。条状模型在相关文献中被很多研究人员使用, 并被证实该替代方法是可行的^[4-6]。同时, 要对剖面施加相应的约

束。

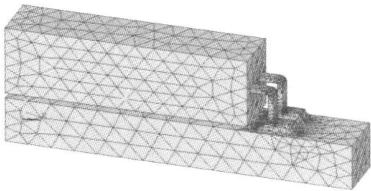


图 2 焊点网格模型

Fig. 2 Meshed model of soldered joints

1.2 材料参数的选择

QFP 模型的上下两层材料均认为是线弹性材料, 并认为其材料性能不受温度的影响, 也即为各向同性的材料, 其主体材料的特性参数如表 3 所示。为了使模拟计算结果更为准确地反映实际情况, 可以借 SnPb 的粘塑性模型, 即 Anand 方程, 相关参数如表 4^[7]。

表 3 线弹性材料特性参数

Table 3 Natural parameters of elastic materials

材料	弹性模量 <i>E</i> /GPa	泊松比 γ	线膨胀系数 $\alpha_l/(10^{-6} \cdot ^\circ\text{C}^{-1})$
封装塑料	12.513	0.25	15
铜引线	117	0.30	16.6
Sn63Pb37	33.58	0.40	25
FR-4	11	0.28	15

表 4 Sn63Pb37 钎料 Anand 方程的材料参数

Table 4 Material parameters in viscoplastic Anand equation for Sn63Pb37 solder

常数 <i>A</i> /s ⁻¹	气体常数 <i>R</i> /(J·K ⁻¹ ·mol ⁻¹)	激活能 <i>Q</i> /(J·mol ⁻¹)	应力乘子 ξ	敏感指数 <i>m</i>	系数 <i>S</i> /MPa	指数 <i>n</i>	硬化常数 <i>h</i> ₀ /MPa	应变指数 <i>a</i>	形变阻抗 <i>S</i> ₀ /MPa
6 220	8.314	54 258	3.33	0.27	36.86	0.022	60 599	1.781 1	3.152 2

1.3 温度的加载

为了计算的精确性, 对 QFP 模型施加边界条件: PCB 板底面施加刚性零约束, PCB 板与封装塑料基板的最里侧面分别施加 *x* 方向零位移刚性载荷。由于电子产品的工作状态都是在交变温度的环境下进行的, 所以在加载温度时, 用的是循环交变温度载荷。热场分析所采用的加载方式为温度加载, 文中按照美国的军用标准 ML-STD-883 进行, 采用温度为 218~398 K, 高低保温时间为 25 min, 升温速率为 20 K/min, 热循环周期为 68 min, 共进行 5 个循环, 且假设模型在 298 K 时, 其内部的热应力为零, 温度循环如图 3 所示。

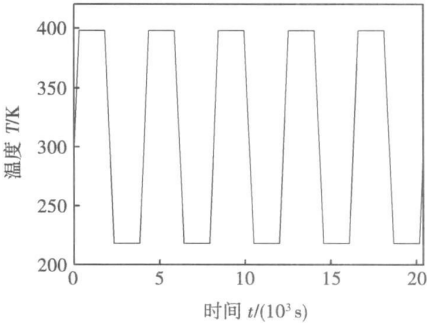


图 3 温度载荷曲线图

Fig. 3 Loading specification of temperature cycles

2 模拟结果和分析

加载完成后,可以求解出QFP器件焊点的应力分布图,如图4所示,由于温度循环载荷以及焊点和PCB板之间的线膨胀系数差异共同作用而导致焊点局部区域出现应力集中,且随着温度循环做周期性的变化^[8]。从图4中可以看出,焊点根部、焊趾部位以及引线 and 焊点交界处为应变集中区域,该三处将可能成为焊点发生破坏区域,焊点的这三处区域呈高应力应变状态,是焊点的薄弱环节,焊点裂纹将最先在此处产生并且扩展,最后因断裂而失效。又由图4可以看出,焊点根部、焊趾部位以及引线 and 焊点交界处的尖端均为应力集中的区域,在焊点根部的应力值是最大的,而焊点所受到的应力主要是引线和PCB板的拉应力,其值越大此处越容易发生破坏,所以在焊点根部最容易产生裂纹,从而发生疲劳破坏。该现象在相关文献中已有模拟和试验验证^[9,10]。

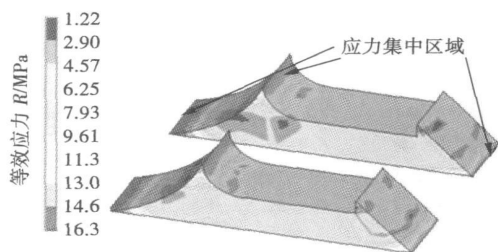


图4 焊点应力云图

Fig. 4 Distribution of soldered joints stress

图5为相同引线数目的不同封装类型QFP的焊点应力随时间变化曲线图,从图中可以看出,TQFP64的焊点等效应力最小,VQFP64焊点次之,SQFP64的焊点等效应力最大。说明在5个热循环完成后,TQFP64的对应焊点的残余应力最小,应力集中最小。这是因为随着引线宽度的增加,整个引线的刚度随之增大,对位移的缓冲作用减小,传递到焊点的应力相应增大,导致焊点的等效应变值增加;与此同时,由于引线宽度的增加导致引线的刚度随之增大,各引线及焊点之间的约束度增加,相应就会导致应力值变大^[11]。另外,随着引线间距的增加,引线对器件的机械支持作用降低,引线易发生变形,产生破坏,所以焊点的等效应力随着引线间距的增大而增大。另有研究表明^[12],当引线的高度等于0.7 mm左右时存在一个焊点的最大值,当引线焊点

小于或大于0.7 mm时,焊点应力均减小。模拟结果与已有的结论都相吻合。

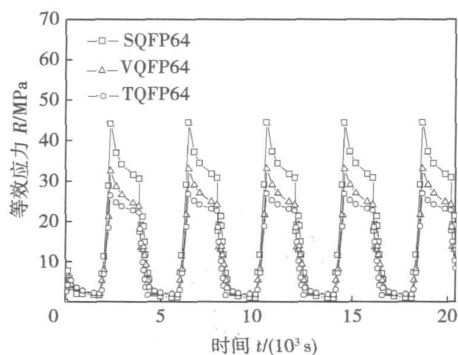


图5 焊点应力曲线

Fig. 5 Stress curved diagrams of soldered joints

图6为引线间距相同时的QFP的焊点应力随时间变化曲线图,从图6中可以看出,QFP32的焊点等效应力最大,QFP64的焊点等效应力最小,QFP44焊点居中。当引线间距一定时,对于QFP器件而言,引线宽度越小,单位面积的抗拉强度越大,对应的焊点强度就越高。此外,引线的高度以及与焊盘接触的长度对焊点应力也有影响。由图可知,在循环加载的过程中,由于残余应力累积的原因,应力具有迭加性。结合温度加载图可以看出,从高温向低温变化阶段,呈现应力增加变化的趋势;另外,在高温阶段出现了应力松弛,当高温保温阶段结束时,应力松弛几乎接近于零,而低温保温阶段并没有明显的应力松弛。

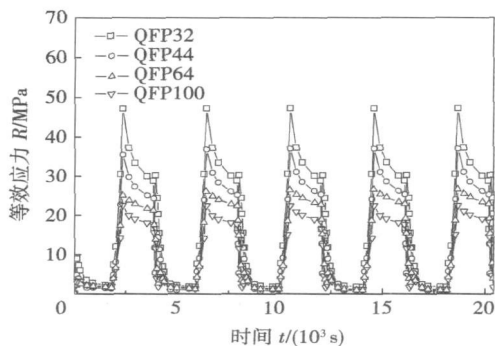


图6 应力曲线图

Fig. 6 Stress curved diagrams

比较间距为0.5 mm的QFP100和间距为0.8 mm的QFP32, QFP44和QFP64可知,QFP100焊点的

应力最小, 已有研究表明^[13,14], QFP 器件的抗拉强度与 QFP 的引脚焊接面积成反比, 即引线宽度和间距越小, 焊点的抗拉强度也越高, 从而验证了高密度细引脚 QFP 器件的可靠性更高, 可以为实际的应用提供一定的理论依据。

3 结 论

(1) 对于 QFP 器件, 其应变的主要区域集中在焊点根部、焊趾部位以及引线和焊点交界处, 而在此三个区域中, 焊点根部的应力值是最大的, 所以在焊点根部最容易产生裂纹, 从而发生疲劳破坏。此外, 在循环加载的过程中, 由于残余应力累积的原因, 应力具有迭加性。

(2) 在引线数目相同的情况下, SQFP64, TQFP64 和 VQFP64 三种类型封装器件中, TQFP64 焊点的等效应力最小, 最不容易产生裂纹, 焊点的破坏可能性最小。

(3) 在引线间距相同的情况下, QFP32, QFP44 和 QFP64 三种器件中, QFP64 焊点的应力和应变最小, 而 QFP32 应力和应变最大, 最容易发生疲劳破坏。同时与 QFP100 比较可知, 高密度细间距引脚的焊点可靠性更高。

参考文献:

[1] 王 考, 陈 循, 褚卫华. 温度循环应力剖面对 QFP 焊点热疲劳寿命的影响[J]. 计算机力学学报, 2005 22(4): 170—175.
[2] 韩宗杰, 薛松柏, 王俭辛, 等. QFP 器件半导体激光钎焊焊点力学性能和显微组织[J]. 焊接学报, 2006, 27(10): 41—44.
[3] 钱乙余, 马 鑫, 吉田综仁. 表面组装焊点内部应力—应变

场的数值模拟(II)[J]. 中国有色金属学报, 2000, 10(3): 411—415.
[4] Lau J, Daukser W, Clara S, *et al.* Effects of ramp-time on thermal fatigue life of SnAgCu lead-free solder joints[C] // Electronic Components and Technology Conference, Lake Buena Vista, FL, 2005.
[5] Schmidt C G, Simons J W, Kanazawa C H, *et al.* Thermal fatigue behavior of J-lead solder joints[J]. IEEE Transactions on Components, Packaging, and Manufacture Technology Part A, 1995, 18(3): 611—617.
[6] Lau J, Dauksher W. Reliability of an 1657CCGA (ceramic column grid array) package with 95.5Sn3.9Ag0.6Cu lead-free solder paste on PCBs (printed circuit boards)[J]. Journal of Electronic Packaging, 2005, 127(2): 96—105.
[7] 王 莉, 陈 旭, Nose H, 等. Anand 模型预测 63Sn37Pb 焊锡钎料的应力应变行为[J]. 机械强度, 2004, 26(4): 447—450.
[8] 薛松柏, 吴玉秀, 崔国平, 等. 热循环对 QFP 焊点强度及其微观组织影响规律的数值模拟[J]. 焊接学报, 2006, 27(11): 1—4.
[9] 张 亮, 薛松柏, 卢方焱, 等. 不同钎料对 QFP 焊点可靠性影响的有限元分析[J]. 焊接学报, 2007, 28(10): 45—48.
[10] Lau J, Pao Y H, Larner C, *et al.* Reliability of 0.4 mm pitch, 256—pin plastic quad flat pack no-clean and water-clean solder joints [C] // Electronics Components and Technology Conference, Orlando, FL, USA, 1993.
[11] 吴玉秀, 薛松柏, 张 玲, 等. QFP 组件的优化模拟及焊点热疲劳寿命的预测[J]. 焊接学报, 2006, 27(8): 99—102.
[12] 吴玉秀, 薛松柏, 胡永芳. 引线尺寸对 CPGA 翼形引线焊点可靠性的影响[J]. 焊接学报, 2005, 26(10): 105—108.
[13] 胡永芳, 薛松柏, 禹胜林. QFP 结构微焊点强度的试验[J]. 焊接学报, 2005, 26(10): 78—80.
[14] 薛松柏, 吴玉秀, 韩宗杰, 等. 不同引线数 QFP 器件焊点等效应力的数值模拟[J]. 焊接学报, 2007, 28(6): 17—20.

作者简介: 盛 重, 男, 1984 年出生, 硕士研究生。主要从事微电子焊接及无铅钎料研究。

Email: orochiai@126.com

[上接第 84 页]

功率大于 13 kW 时随着焊缝熔深的增加斜率明显减小; 焊透对接焊缝形状为 Y 形, 送丝速度和焊缝间隙对 Y 形焊缝形态影响很大, 送丝速度越快, 焊缝上半部梯形宽度 D 越大, 同时上半部焊缝的高度 H 相应减小, 而下半部焊缝宽度 d 基本与单激光焊时相同, 激光的熔深随着送丝速度的增大而有所减小, 焊缝间隙越大, 焊缝上半部分梯形高 H 与宽 D 越大, 而且熔池运动越充分, 这有利于熔池中气体的排出。

参考文献:

[1] Salminen A. The effects of filler wire feed on the efficiency of laser

welding[J]. First International Symposium on High-Power Laser Macroprocessing Isamu Miyamoto. Proceedings of the SPIE, 2003, 48(31), 263—268.
[2] Steen, William M. Laser material processing[M]. 3rd edition. London, New York, Springer, 2003.
[3] 陈彦宾. 现代激光焊接技术[M]. 北京: 科学出版社, 2005.
[4] Stauffer Herbert. Laser—hybrid welding of ships[J]. Welding Journal, 2004, 83(6): 39—43.
[5] 张永康. 激光加工技术[M]. 北京: 化学工业出版社, 2004.
[6] 倪 宇. 激光电弧复合焊接及激光焊接超低碳钢的焊缝磁性研究[D]. 武汉: 华中科技大学, 2004.

作者简介: 唐 卓, 男, 1983 年出生, 硕士研究生。研究方向为大功率激光焊接工艺。发表论文 2 篇。

Email: tangzhuo1983@sjtu.edu.cn

results with material coupling of Q235—Q235 indicate that the temperature distribution on the friction surface has a tendency to rise gradually from the inside to outside on radial direction during welding process, while the contact pressure distribution decreases gradually. With the increase of rotary speed, the temperature is remarkably increased while the material doesn't illustrate obvious plastic deformation, but the effect is relatively weak with the increase of temperature. When material in the contact zone illustrates plastic strain at high temperatures, increasing axial force is more effective for increasing temperature and inducing large deformation.

Key words: friction hydro pillar processing; friction stitch welding; finite element method; thermal-mechanically coupled analysis

Mechanical properties and welding parameters window of friction stir welding

WANG Wei, SHI Qingyu, LI Ting, LI Hongke (Advanced Materials Processing Technology, Ministry of Education, Tsinghua University, Beijing 100084, China). p77—80

Abstract: Friction stir welding parameters play an important role of figuration and mechanical properties of welded joint. In this study, the 3 mm plate of 2024 aluminum alloy was selected as base metal. By operating a great deal of butt welding experiments, the quality of welded joint under various parameters was tested. Furthermore, the welding parameters window was established. In the parameter of rotation speed 375—475 r/min and welding speed 150—235 mm/min, the tensile strength of welded joint can be higher than 80% of the one of base metal. By analyzing the tensile fracture, at the upper district of joint, the material had good plastic aspect, while the lower district was worse than the upper one. The joint showed distinct layers along the depth.

Key words: friction stir welding; aluminum alloy; mechanical property; welding parameters window; fracture

Technological effect on bead characteristics of homemade thick plate welded by high power laser with filler wire

TANG Zhuo, ZHAO Lianglei, CAI Yan, WU Yixiong (School of Materials Science & Engineering, Shanghai Jiaotong University, Shanghai, 200240, China). p81—84, 88

Abstract: The high power density of laser makes laser welding process become one of the most promising and efficient welding method. The high power laser welding with filler wire of 10 mm and 12 mm thick plates was studied, and the plasma behavior was analyzed as well. The results showed when the laser power is over 13 kW, the penetration curve becomes gentler and the gradient declines obviously. However, in regard to the fully-penetrated seam, it could not fully demonstrate the effects of the welding parameters on the cross-section only with width and penetrations of the weld bead. The cross-section of fully-penetrated bead appears to be a Y shape. And this kind of Y shape is further designed to be a combination with an inverted trapezoid on the top and a rectangle below. In this way, wire feeding rate and gap are varied in order to study their effects on the Y shape bead dimensions while laser power and welding speed keeping constant. In addition, the influence of plasma of the protective gas was studied.

Key words: homemade thick plate; high power laser; laser welding with filler wire; weld appearance

Effect of leads pitch on soldered joint reliability of QFP device with finite element analysis

SHENG Zhong, XUE Songhai, ZHANG Liang, GAO Lili (College of Materials Science and Technology, Nanjing University of Aeronautics and Astronautics, Nanjing 210016, China). p85—88

Abstract: Finite element method was used to simulate the residual stress in soldered joints of QFP device with the same distance and number of leads, respectively. The results indicated that the stress concentration areas in soldered joint locate at the heel and toe of the soldered joint, as well as at the area between the lead and the soldered joint; the largest value of the stress was in the heel of the soldered joints, which would be the weakest area of the joints. Through the comparison of these results, especially the analysis of stress curves, it was shown that stress increased periodically due to the accumulation of residual stress. In the QFP device with the same number of lead, the stress was increasing in the order: TQFP64 < VQFP64 < SQFP64. In the QFP devices with the same distance of leads, the increasing of stress was in the order: QFP64 < QFP44 < QFP32. Comparing with QFP100 at the same time, it was shown that the soldered joint reliability of high density fine pitch device is more qualified.

Key words: finite element method; residual stress; distance of lead; number of lead

Investigation on process optimization of Cu/Ti electron beam welding

LIU Wei, CHEN Guoqing, ZHANG Binggang, FENG Jicai (State Key Laboratory of Advanced Welding Production Technology, Harbin Institute of Technology, Harbin 150001, China). p89—92

Abstract: QCr0.8/TC4 electron beam welding process and the structure of joints were studied. The melting quantity of Cu alloy was lower due to its high thermal conductivity; moreover, there were lots of brittle intermetallic compounds in the weld, so the tensile strength of the joint was low. The non-centered electron beam welding was used to improve the tensile strength of Cu/Ti joints. It was indicated that the tensile strength was increasing as the lateral deviation quantity increasing, and the maximum value, 270.5 MPa was obtained when the lateral deviation quantity was 0.8 mm. The fracture occurred near TC4 side, and it was quasi-cleavage crack. The weld was consisted of fusion zone and reaction layer near TC4 side. The fusion zone was mainly consisted of Cu-based solid solution with lower hardness than TC4. In the reaction layer, the component transition was obvious, and there were lots of intermetallic compounds. The thickness of the reaction layer was changed as the process parameter being varied, which influenced the mechanical properties of the joint.

Key words: QCr0.8 alloy; TC4 alloy; electron beam welding; process optimization

Microstructures and properties in simulated heat-affected zone of copper bearing age-hardening steel

LIU Wenyan^{1,2}, WANG Lai¹, LIU Jibin², ZHANG Yunyan², LI Pinghe², YUAN